Spans of Polymer Chains Measured with Respect to Chain-Fixed Axes

Robert J. Rubin* and Jacob Mazur

Institute for Materials Research, National Bureau of Standards, Washington, D.C. 20234. *Received July 8, 1976*

ABSTRACT: An N-step random walk on a cubic lattice is adopted as a model of a polymer chain. The span or extent of a random walk in a direction **e** is defined as the maximum distance between parallel planes normal to **e** which contain lattice points visited by that walk. The spans of each random walk configuration are measured with respect to two different sets of orthogonal axes determined by the configuration. The first set of orthogonal axes is based on the direction of the maximum span of the configuration. The second set is based on the directions of the principal components of the radius of gyration tensor of the chain configuration. For each set of axes, a smallest right prism is determined whose edges are parallel to the chain-fixed axes and which contain all the steps of the random walk. A Monte Carlo procedure is used to estimate the average largest, intermediate, and smallest spans, or prism dimensions. Both the simple unrestricted random walk with N = 50, 100, 200 and the self-avoiding random walk with N = 50, 75, 100, 150 are treated. In the case of the orthogonal axes based on the maximum span, the ratio of the average maximum span to the average smallest span is approximately independent of N and equal to 2.42 for the unrestricted walk and 2.73 for the self-avoiding walk. The distribution of steps inside the spanning right prisms is investigated by dissecting them in two different ways. First, the prism is cut in ten equal sections by a set of parallel, equally spaced planes which are normal to an edge of the prism. The fraction of steps contained in pairs of sections which are equidistant from the central cutting plane is determined. This procedure is repeated in turn for each of the different edges of the prism. Second, a symmetric oval (the ellipsoid is a special case) is inscribed in the prism with its axes parallel to those of the prism. Four similar and successively smaller nested ovals are also introduced. For each random walk configuration, the fraction of steps contained in each oval shell is determined.

I. Introduction

In this paper we continue our investigation of the spans of unrestricted and self-avoiding cubic-lattice-random-walk models of polymer chains.[1] The two terms, random walk and random polymer chain, are used interchangeably as are the terms step and polymer segment. The span of an N-step random walk in a direction **e** is defined as the maximum distance between parallel planes normal to **e** which contain lattice points visited by that walk. In the preceding paper,[1] RMI, the spans of each random walk are determined with respect to the directions of the principal axes of the cubic lattice, x_1, x_2, and x_3. The span in the x_i direction is denoted by $X_i(N)$ and the values of these spans are ordered according to their magnitude. The ordered spans are denoted by the symbol $\xi_i(N)$ where $\xi_3(N) \geq \xi_2(N) \geq \xi_1(N)$. These three spans, $\xi_i(N)$, i = 1, 2, 3, define the dimensions of the smallest right prism, $\Pi_x(N)$, whose edges are parallel to the x_i axes and which contains all the steps in the random walk. One of the principal results obtained in RMI is that the right prism whose edges have the lengths $\langle\xi_3(N)\rangle$, $\langle\xi_2(N)\rangle$, and $\langle\xi_1(N)\rangle$ is significantly noncubic where $\langle\xi_i(N)\rangle$ denotes the average value of $\xi_i(N)$. The relative proportions, $\langle\xi_3(N)\rangle:\langle\xi_2(N)\rangle:\langle\xi_1(N)\rangle$ in the limit $N \to \infty$ are 1.637:1.267:1 in the case of the unrestricted random walk and 1.75:1.31:1 in the case of the self-avoiding random walk. This result, that the typical or average shape of a polymer chain is asymmetric, is not new. Kuhn[2] presented approximate arguments leading to a similar conclusion over 40 years ago. Hollingsworth[3,4] and later Weidmann, Kuhn, and Kuhn[5] elaborated on these same arguments. More recently, Koyama,[6,7] Solč and Stockmayer,[8] and Solč[9] used Monte Carlo methods to investigate the principal components of the moment of inertia tensor, or radius of gyration tensor, of an unrestricted random walk. Solč and Stockmayer found that the relative values of the average ordered principal components were 11.69:2.69:1 for N = 50 and 100. Mazur, Guttman, and McCrackin[10] have extended these calculations to the case of self-avoiding random walks and have obtained for the corresponding relative proportions 14.81:3.07:1. In the dilute solution properties of random chain polymer molecules, there are many immediate and obvious physical consequences of the asymmetric dimensions of the average spanning prism of the typical molecule. Proper account of the asymmetry must be taken in all experiments involving motion of the entire chain or parts of it, relative to the solvent such as experiments on viscosity, streaming birefringence, dielectric relaxation, and rates of sedimentation and diffusion. The average dimensions of the spanning prism also figure in theoretical models of peak migration in gel permeation chromatography.

The spans in RMI are measured with respect to the space-fixed lattice directions, x_1, x_2, x_3. In the present paper, we investigate the spans with respect to directions determined by the random walk configuration itself. In this way we can obtain more explicit and detailed information regarding the asymmetric shape of polymer chains. Two different sets of orthogonal chain-fixed directions are considered. The first set, based on the direction of the maximum span of the random walk, is defined as follows. Consider the set of all arbitrarily oriented rectangular prisms with minimum dimensions which contain the random walk. Determine the subset of prisms which has the longest edge. The edge length, $R_3(N)$, is the maximum span of the random walk configuration. Then for this subset determine the prism(s), $\Pi_R(N)$, with the next longest edge and denote this edge length by $R_2(N)$. The third edge length, $R_1(N)$, is the smallest span associated with the direction of the maximum span $R_3(N)$ and $R_2(N)$. Note that the direction associated with the maximum span may not be unique. That is, two different pairs of steps in the random walk configuration might be separated by the same distance, $R_3(N)$. Note also that the smallest span $R_1(N)$, which is associated with $R_3(N)$, is not necessarily the minimum span of the random walk configuration. The second set of orthogonal chain-fixed directions which we consider is the set associated with the directions of the principal axes of inertia of the chain. First, the principal components of the radius of gyration and the directions of the principal components are determined for the chain. Then the principal components of the square radius of gyration are ordered according to their magnitude. The jth ordered component of the square radius of gyration is denoted by $S_j^2(N)$, j = 1, 2, 3, and $S_3^2(N) \geq S_2^2(N) \geq S_1^2(N)$. The

* National Institutes of Health, Bethesda, Md. 20014.

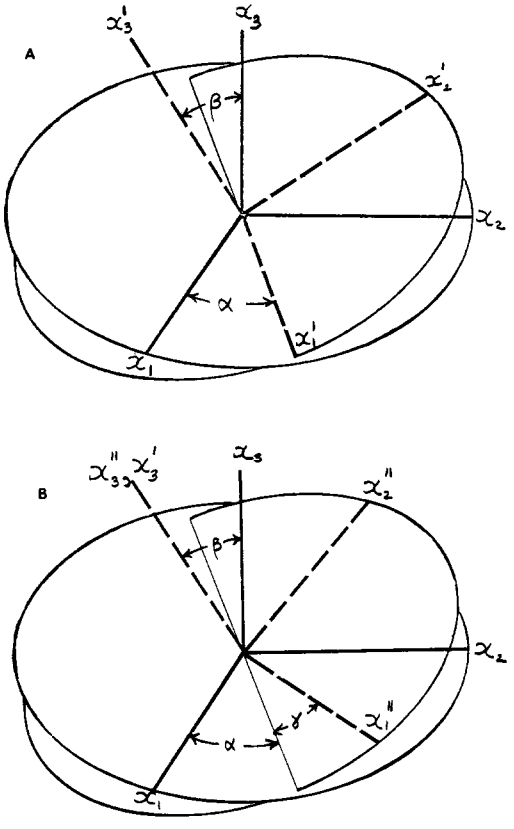

Figure 1. (A) The two sets of orthogonal axes $\{x_1, x_2, x_3\}$ and $\{x_1', x_2', x_3'\}$ are shown as well as the angles α and β. (B) The two sets of orthogonal axes $\{x_1, x_2, x_3\}$ and $\{x_1'', x_2'', x_3''\}$ are shown as well as the angles α, β, and γ.

span, $r_j(N)$, in the direction of the jth ordered component, $S_j^2(N)$, is determined for each principal direction. In this way, a smallest rectangular prism, $\Pi_r(N)$, whose edges are parallel to the directions of the principal axes of inertia is determined for each random walk configuration.

In section 2 we describe a Monte Carlo procedure for calculating estimates of the first and second moments of the spans $R_i(N)$, $i = 1, 2, 3$, of unrestricted and self-avoiding walks. Estimated values of the first and second moments are obtained for the unrestricted random walk ($N = 50, 100, 200$) and the self-avoiding walk ($N = 50, 75, 100, 150$). In section 3 we describe an analogous procedure for the calculation of the first and second moments of the spans $r_i(N)$, $i = 1, 2, 3$, associated with the ordered principal components of the square radius of gyration. In this case, estimated values of the moments are presented for unrestricted ($N = 50, 100, 200$) and self-avoiding ($N = 50, 75, 100, 150$) walks.

In addition to determining the ordered dimensions of a minimum-size right prism, $\Pi_r(N)$ or $\Pi_R(N)$, which contains all polymer chain segments, we investigate the distribution of segments inside these right prisms by dissecting them in two different ways. First, the prism is cut in ten sections by a set of parallel, equally spaced planes which are normal to an edge of the prism. The number of polymer segments contained in the pairs of sections which are equidistant from the central cutting plane is determined. This procedure is repeated in turn for each of the different edges of the prism. The three segment density distributions which are obtained in this way for the case of the prisms, $\Pi_r(N)$, can be used to reconcile an apparent discrepancy between the relative values obtained for $\langle S_j^2(N)\rangle$, $j = 1, 2, 3$, by Koyama,[6,7] Solč and Stockmayer,[8] Solč,[9] and Mazur, Guttman, and McCrackin[10] and the relative values of the squares of the spans in the corresponding directions. Second, we have introduced a different type of subdivision of the spanning prism. A symmetric oval (the ellipsoid is a special case) is inscribed in the prism with its axes parallel to those of the prism. Four similar and successively smaller nested ovals are also introduced. For each random walk configuration, the fraction of segments contained in each oval shell is determined.

The foregoing calculations of a minimum-size right prism which contains all segments of a given random walk as well as the calculation of the distribution of segments within the right prism have been carried out for both unrestricted random-walk and self-avoiding-random-walk models of polymer chains. As in RMI, the self-avoiding walks are generated by using the method of Rosenbluth and Rosenbluth[11] which is also described in detail in papers by Mazur and McCrackin[12] and McCrackin, Mazur, and Guttman.[13] In this method, the estimated sample average of a physical parameter generally differs from the true average. This difference, or bias, is negligible in a sufficiently large sample.[14,15] The magnitude of the bias in our calculations is discussed in Appendix A, using the average maximum span $\langle R_3(N)\rangle$ as an example.

2. Spans Associated with the Maximum Span

Consider the set of spans measured with respect to chain-fixed axes which is based on the maximum span. In an N-step random walk which starts at the origin of a simple cubic lattice, the coordinates of the jth step are denoted by the vector $\mathbf{x}(j)$ whose components are $x_1(j), x_2(j), x_3(j)$ with $0 \leq j \leq N$ and $x_1(0) = x_2(0) = x_3(0) = 0$. The maximum span, $R_3(N)$, is the maximum distance in the set of $\frac{1}{2}N(N+1)$ inter-step distances,

$$\{[x_1(j) - x_1(k)]^2 + [x_2(j) - x_2(k)]^2 + [x_3(j) - x_3(k)]^2\}^{1/2} \qquad 0 \leq j < k \leq N \tag{1}$$

The direction associated with $R_3(N)$ is the direction of the vector $\mathbf{x}(j') - \mathbf{x}(k')$ connecting the pair of maximally separated steps. If there is not a unique maximum, that is, if more than one pair of steps is associated with $R_3(N)$, then the direction associated with one of the pairs is arbitrarily selected. To determine the maximal spans of the random walk in directions orthogonal to $\mathbf{x}(j') - \mathbf{x}(k')$, we express the $x_1(j), x_2(j), x_3(j)$ coordinates in a new coordinate system x_1', x_2', x_3' where the positive x_3' direction coincides with the direction of $\mathbf{x}(j') - \mathbf{x}(k')$. The transformation of coordinates, specified in terms of the two angles α and β depicted in Figure 1, has the form

$$\begin{pmatrix} x_1'(j) \\ x_2'(j) \\ x_3'(J) \end{pmatrix} = \begin{pmatrix} \cos\alpha & \sin\alpha & 0 \\ -\sin\alpha\cos\beta & \cos\alpha\cos\beta & \sin\beta \\ \sin\alpha\sin\beta & -\cos\alpha\sin\beta & \cos\beta \end{pmatrix} \times \begin{pmatrix} x_1(j) \\ x_2(j) \\ x_3(j) \end{pmatrix} \tag{2}$$

where $x_i'(j)$ is the coordinate of particle j in the x_i' direction. The maximum span in a direction transverse to $\mathbf{x}(j') - \mathbf{x}(k')$, $R_2(N)$, is the maximum transverse distance in the set of $\frac{1}{2}N(N+1)$ distances

$$\{[x_1'(j) - x_1'(k)]^2 + [x_2'(j) - x_2'(k)]^2\}^{1/2} \qquad 0 \leq j < k \leq N \tag{3}$$

The direction associated with $R_2(N)$ is the direction of the vector whose components are $\{x_1'(j'') - x_1'(k''), x_2'(j'') - x_2'(k''), 0\}$ where steps j'' and k'' have the maximum transverse separation. Finally, the $x_1'(j), x_2'(j), x_3'(j)$ coordinates are transformed to a new coordinate system by a simple rotation in the x_1', x_2' plane ($x_3' = 0$). In the new

Table I
Monte Carlo Estimates for Spans of Random Walks which are Based on the Maximum Span

N	$\langle R_1(N)\rangle$	$\langle R_2(N)\rangle$	$\langle R_3(N)\rangle$	$\langle R_1^2(N)\rangle$	$\langle R_2^2(N)\rangle$	$\langle R_3^2(N)\rangle$	No. of configurations
			(A) Unrestricted				
50	3.4626	5.1962	8.7137	12.445	27.915	80.408	2000
75	4.3681	6.5262	10.615	19.839	44.190	119.03	800
100	5.1994	7.6256	12.559	27.961	60.185	166.80	2000
150	6.5648	9.5281	15.522	44.676	94.147	253.62	800
200	7.5447	11.074	18.079	58.803	126.70	344.81	1500
			(B) Self-Avoiding				
50	4.524	7.020	12.582	21.253	50.736	164.38	7200
75	5.901	9.144	16.086	36.019	86.022	269.85	8800
100	7.195	10.975	19.328	53.555	124.02	389.48	7200
150	9.169	14.382	25.118	86.571	213.86	656.95	8800

coordinate system the positive direction of the two-component vector $x_1'(j'') - x_1'(k''), x_2'(j'') - x_2'(k'')$ coincides with the positive x_2'' direction. The transformation of coordinates, specified in terms of the angle γ, which is shown in Figure 1B, has the form

$$\begin{pmatrix} x_1''(j) \\ x_2''(j) \\ x_3''(j) \end{pmatrix} = \begin{pmatrix} \cos\gamma & \sin\gamma & 0 \\ -\sin\gamma & \cos\gamma & 0 \\ 0 & 0 & 1 \end{pmatrix} \begin{pmatrix} x_1'(j) \\ x_2'(j) \\ x_3'(j) \end{pmatrix} \quad (4)$$

The third span, $R_1(N)$, associated with $R_3(N)$ (and the direction $\mathbf{x}(j') - \mathbf{x}(k')$) is the maximum in the set

$$|x_1''(j) - x_1''(k)|$$
$$0 \leq j < k \leq N \quad (5)$$

In addition to the maximal set of spans $R_1(N), R_2(N), R_3(N)$ whose calculation we have outlined, there is an analogous set of minimal spans based on the smallest span of a random-walk configuration. However, we have not attempted to study the minimal set because the search for the minimum edge length of *all* right prisms which contain a given random walk is considerably more lengthy than the calculation of the maximum edge length outlined above.

Monte Carlo estimates of the average values of $R_i(N)$ and $R_i^2(N)$ for $i = 1, 2, 3$ and $N = 50, 75, 100, 150, 200$ are listed in Table IA for unrestricted random walks. The last column in the table lists the number of random-walk configurations on which the Monte Carlo estimates are based. Table IB contains the corresponding quantities for self-avoiding walks. The magnitude of the bias which is introduced by the method of Rosenbluth and Rosenbluth[11] in these Monte Carlo estimates is discussed in Appendix A. Some noteworthy aspects of the results obtained in Tables IA and IB which are discussed in the remainder of this section are: (i) the distribution function of $R_i(N)$, the average value, $\langle R_i(N)\rangle$, and the root-mean-square dispersion $\sigma[R_i(N)] = [\langle R_i^2(N)\rangle - \langle R_i(N)\rangle^2]^{1/2}$ for $i = 1, 2, 3$; (ii) the relative proportions, $\langle R_3(N)\rangle/\langle R_1(N)\rangle$ and $\langle R_2(N)\rangle/\langle R_1(N)\rangle$; and (iii) the comparison of the values of $\langle R_i^2(N)\rangle$ with the mean-square end-to-end distance $\langle l^2(N)\rangle = \langle x_1^2(N) + x_2^2(N) + x_3^2(N)\rangle$.

(i) The Distribution Functions of the Spans $R_i(N)$, $i = 1, 2, 3$. In addition to determining the average values, $\langle R_i(N)\rangle$, displayed in Tables IA and IB, the distribution of values of $R_i(N)$ for walks of each length was determined. A set of typical results for the self-avoiding walk is displayed in Figure 2 where histograms of values of $R_i(150)$, $i = 1, 2, 3$, are plotted. The abscissa scale is span measured in units of the nearest neighbor lattice spacing. The ordinate scale is the fraction of random walk samples per unit length of the span

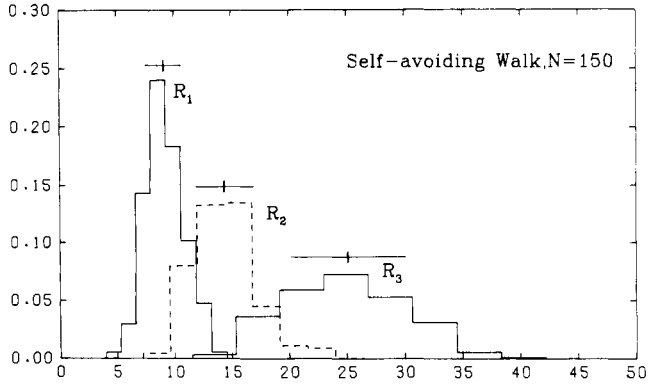

Figure 2. Histograms showing the distribution of values of $R_i(150)$, $i = 1, 2, 3$, for the self-avoiding walk. The abscissa scale is measured in units of the nearest neighbor lattice spacing. The ordinate scale is the fraction of random walk samples per unit length of the span for which the span $R_i(150)$ falls in the interval specified on the abscissa. The average values, $\langle R_i(150)\rangle$, associated with the histograms are indicated by vertical tick marks above the peak values. The range of values defined by the interval $\langle R_i(150)\rangle - \sigma[R_i(150)] \leq R_i(150) \leq \langle R_i(150)\rangle + \sigma[R_i(150)]$ is indicated for each histogram by a horizontal line through the associated tick mark.

for which the span $R_i(150)$ falls in the range specified on the abscissa. Consequently, the area under each of the three histograms is unity. Similar histograms for other values of N and for the unrestricted random walk have the same qualitative form as that shown in Figure 2. The average value, $\langle R_i(150)\rangle$, associated with each of the histograms in Figure 2 is indicated by a vertical tick mark above the peak value of the distribution function. The range of values of $R_i(150)$ defined by the interval $\langle R_i(150)\rangle - \sigma[R_i(150)] \leq R_i(150) \leq \langle R_i(150)\rangle + \sigma[R_i(150)]$ is indicated for each distribution function by a horizontal line through the corresponding tick mark. The reduced mean-square deviations of these distributions, $[\langle R_i^2(N)\rangle - \langle R_i(N)\rangle^2]/\langle R_i(N)\rangle^2$, fall in the range of 0.03 to 0.06, giving further evidence of the sharpness of these distributions.

(ii) The Relative Proportions $\langle R_3(N)\rangle/\langle R_1(N)\rangle$ and $\langle R_2(N)\rangle/\langle R_1(N)\rangle$. The relative proportions, $\rho_3(R;N) = \langle R_3(N)\rangle/\langle R_1(N)\rangle$ and $\rho_2(R;N) = \langle R_2(N)\rangle/\langle R_1(N)\rangle$, are plotted vs. N^{-1} in Figure 3 for both the case of the unrestricted and the self-avoiding random walk. The qualitative behavior in the two cases is similar. There appears to be a weak dependence of these proportions on N^{-1}. If this dependence of $\rho_3(R;N)$ and $\rho_2(R;N)$ on N^{-1} is ignored, the average values of $\rho_3(R;N)$ and $\rho_2(R;N)$, $\overline{\rho_3(R)}$ and $\overline{\rho_2(R)}$, can be computed. For self-avoiding walks, the following average relative proportions are obtained:

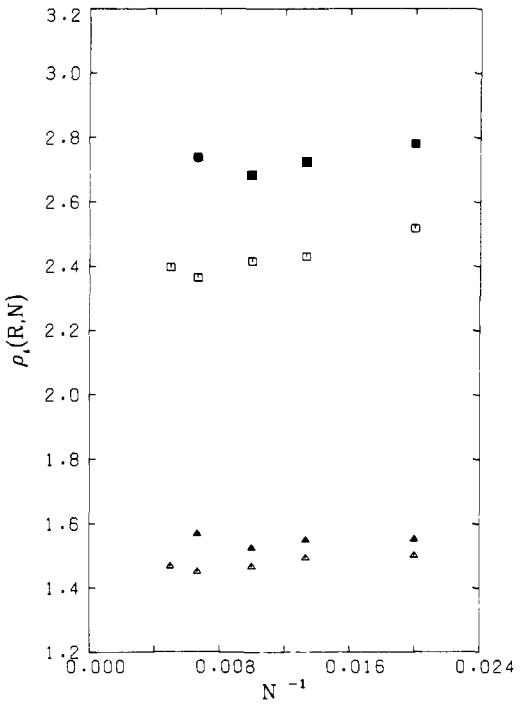

Figure 3. The relative proportions, $\rho_3(R;N) = \langle R_3(N)\rangle/\langle R_1(N)\rangle$ and $\rho_2(R;N) = \langle R_2(N)\rangle/\langle R_1(N)\rangle$, are plotted vs. N^{-1} for both the unrestricted random walk and the self-avoiding random walk. The squares refer to values of $\rho_3(R;N)$ and the triangles to $\rho_2(R;N)$ while the filled symbols refer to the self-avoiding walk and the open symbols to the unrestricted random walk.

$$\overline{\rho_3(R)} = 2.73 \text{ and } \overline{\rho_2(R)} = 1.55 \tag{6}$$

For the unrestricted random walk, the average relative proportions are

$$\overline{\rho_3(R)} = 2.42 \text{ and } \overline{\rho_2(R)} = 1.48 \tag{7}$$

(iii) The Relative Values, $\langle R_i^2(N)\rangle/\langle l^2(N)\rangle$, $i = 1, 2, 3$. In the case of the unrestricted random walk, the values of $\langle R_i^2(200)\rangle$, $i = 1, 2, 3$, given in Table IA divided by the mean-square end-to-end distance, $\langle l^2(200)\rangle = 3\langle x_1^2(200)\rangle = 200$, are

$$\langle R_3^2(200)\rangle/\langle l^2(200)\rangle = 1.72 \tag{8}$$

$$\langle R_2^2(200)\rangle/\langle l^2(200)\rangle = 0.63 \tag{9}$$

and

$$\langle R_1^2(200)\rangle/\langle l^2(200)\rangle = 0.29 \tag{10}$$

Similar values of the ratios are obtained for $N = 50$, 75, 100, and 150. It is clear from the values of these ratios that the direction of the end-to-end vector is correlated with the direction of the maximum span. A similar conclusion in the case of the self-avoiding walk follows from the values of the corresponding ratios

$$\langle R_3^2(150)\rangle/\langle l^2(150)\rangle = 1.50 \tag{11}$$

$$\langle R_2^2(150)\rangle/\langle l^2(150)\rangle = 0.49 \tag{12}$$

and

$$\langle R_1^2(150)\rangle/\langle l^2(150)\rangle = 0.20 \tag{13}$$

where the values of $\langle R_i^2(150)\rangle$ are given in Table IB and the value of $\langle l^2(150)\rangle = 437.10$ is obtained from Table III in RMI.

(iv) The Asymptotic Formulas for $\langle R_3(N)\rangle$ for Unrestricted and Self-Avoiding Walks. In order to derive an asymptotic expression for $\langle R_3(N)\rangle$ from the tabulated values in Table IA for the unrestricted random walk, we have assumed that $\langle R_3(N)\rangle$ has the asymptotic form

$$\langle R_3(N)\rangle = AN^{1/2} + B$$

in analogy with the exact asymptotic form for the span with respect to a space-fixed axis obtained by Daniels[16] and Rubin and Mazur[1]

$$\langle X(N)\rangle = aN^{1/2} - 1$$

The values of A and B have been determined from the values of $\langle R_3(N)\rangle$ in Table IA. The result is

$$\langle R_3(N)\rangle = 1.32N^{1/2} - 0.57$$

It should be noted that Kuhn[17] has asserted that

$$\langle R_3(N)\rangle \sim 1.5N^{1/2}$$

and his assertion has been repeated elsewhere[18] even though *no outline of his calculation has been published.* Our Monte Carlo estimates of $\langle R_3(N)\rangle$ which have been analyzed in the above manner do not support Kuhn's value of $A = 1.5$.

The values of $\langle R_3(N)\rangle$ in Table IB for the self-avoiding walk can be used to obtain a corresponding asymptotic formula. In this case we have assumed that $\langle R_3(N)\rangle$ has the asymptotic form[19]

$$\langle R_3(N)\rangle = \alpha N^{0.61} - 0.57$$

and determined the value of α from the values of $\langle R_3(N)\rangle$ in Table IB. The result is

$$\langle R_3(N)\rangle = 1.19N^{0.61} - 0.57$$

3. Spans Associated with the Ordered Components of the Radius of Gyration Tensor

Next consider the set of chain-fixed spans which is based on the direction of the ordered components of the square radius of gyration tensor, $\mathbf{X}$. The k,l component of the symmetric tensor $\mathbf{X}$ is defined as

$$X_{k,l} = (N+1)^{-1}\sum_{n=0}^{N} x_k(n)\,x_l(n) - (N+1)^{-2}\sum_{n=0}^{N} x_k(n)\sum_{m=0}^{N} x_l(m) \tag{14}$$

The trace of $\mathbf{X}$ equals the square radius of gyration of the polymer chain. The moment of inertia tensor of mechanics, $\mathbf{T}$, is related simply[8,9] to the tensor $\mathbf{X}$,

$$\mathbf{T} = (N+1)\{(X_{11} + X_{22} + X_{33})\,\mathbf{1} - \mathbf{X}\} \tag{15}$$

where $\mathbf{1}$ is the diagonal unit tensor. Thus the directions of the principal axes of inertia coincide with the directions of the principal axes of the square radius of gyration tensor. For a given random walk configuration, it is a straightforward matter to determine the values of $X_{k,l}$ in eq 14 and then the principal components of the gyration tensor and the associated principal axis directions. The principal components of the gyration tensor are ordered according to their magnitude and denoted by $S_3^2(N) \geq S_2^2(N) \geq S_1^2(N)$. The associated orthonormal unit vectors in the principal axis directions are denoted by corresponding subscripts $\mathbf{V}_i = (V_i^{(1)}, V_i^{(2)}, V_i^{(3)})$, $i = 1, 2, 3$, where $V_i^{(k)}$ is the component of $\mathbf{V}_i$ in the x_k direction and $\mathbf{V}_i$ is associated with $S_i^2(N)$. In rare cases where two (or all three) principal components $S_i^2(N)$ are equal, a pair (or triple) of associated orthonormal vectors is arbitrarily chosen.

Having determined a set of principal axis directions for the random-walk configuration, we next introduce a coordinate transformation in which the new origin is located at the center of gravity of the configuration and the directions of the new

Table II
Monte Carlo Estimates for Spans of Random Walks in the Directions of the Ordered Components of the Square Radius of Gyration

N	$\langle S_1^2(N)\rangle$	$\langle S_2^2(N)\rangle$	$\langle S_3^2(N)\rangle$	$\langle r_1(N)\rangle$	$\langle r_2(N)\rangle$	$\langle r_3(N)\rangle$	$\langle r_1^2(N)\rangle$	$\langle r_2^2(N)\rangle$	$\langle r_3^2(N)\rangle$	No. of configurations
					(A) Unrestricted					
50	0.549	1.475	6.495	3.196	4.836	8.458	10.594	24.423	76.173	2000
100	1.081	2.870	12.669	4.768	7.054	12.143	23.528	51.673	156.44	2000
200	2.143	5.595	25.888	7.011	10.161	17.600	50.830	107.19	329.59	1000
					(B) Self-Avoiding					
50	0.973	2.954	14.460	4.065	6.530	12.310	17.167	44.188	159.57	5000
75	1.613	4.751	23.759	5.349	8.457	16.026	29.611	74.071	270.00	3500
100	2.266	6.924	33.158	6.529	10.326	18.847	44.056	110.40	374.93	5000
150	3.693	10.171	53.433	8.553	12.892	24.373	75.804	171.01	620.63	5000

axes, x_1', x_2', x_3', coincide respectively with the directions of $\mathbf{V}_1$, $\mathbf{V}_2$, and $\mathbf{V}_3$. The coordinates of the jth step in the new coordinate system are

$$\begin{pmatrix} x_1'(j) \\ x_2'(j) \\ x_3'(j) \end{pmatrix} = \begin{pmatrix} V_1^{(1)} & V_1^{(2)} & V_1^{(3)} \\ V_2^{(1)} & V_2^{(2)} & V_2^{(3)} \\ V_3^{(1)} & V_3^{(2)} & V_3^{(3)} \end{pmatrix} \begin{pmatrix} x_1(j) - (N+1)^{-1}\sum_{i=0}^{N} x_1(i) \\ x_2(j) - (N+1)^{-1}\sum_{i=0}^{N} x_2(i) \\ x_3(j) - (N+1)^{-1}\sum_{i=0}^{N} x_3(i) \end{pmatrix} \quad (16)$$

and the ith ordered component of the square radius of gyration, $S_i^2(N)$, has the form

$$S_i^2(N) = (N+1)^{-1}\sum_{n=0}^{N} (x_i')^2(n) \quad (17)$$

The span in the direction of $\mathbf{V}_i$ is denoted by $r_i(N)$ and is calculated simply by determining the maximum member of the set

$$\{|x_i'(j) - x_i'(k)|\} \qquad 0 \leq j < k \leq N \quad (18)$$

Monte Carlo estimates of the average values of $r_i(N)$ and $r_i^2(N)$ for $i = 1, 2, 3$ and $N = 50$, 100, and 200 are listed in Table IIA for unrestricted random walks. In addition, the average values of $S_i^2(N)$ are tabulated. The last column in the table lists the number of configurations on which the Monte Carlo estimates are based. Table IIB contains the corresponding quantities for self-avoiding walks.

(i) The Distribution Functions of the Spans $r_i(N)$, $i = 1, 2, 3$. As in the preceding case of spans based on the maximum span, the distribution of values of $r_i(N)$ for walks of each length was determined. A set of results is displayed in Figure 4 where histograms of values of $r_i(150)$, $i = 1, 2, 3$, are plotted for the self-avoiding walk. Corresponding sets of histograms for the unrestricted random walk are qualitatively the same as are the sets of histograms for self-avoiding walks of length $N = 50$, 75, or 100. The unit on the abscissa scale in Figure 4 is the nearest neighbor lattice spacing. The ordinate scale is the fraction of random walks per unit length for which the span $r_i(N)$ falls in the range specified on the abscissa. Consequently the area of each histogram is normalized to unity. The average values, $\langle r_i(150)\rangle$, associated with the histograms in Figure 4 are indicated by vertical tick marks above the peak values of the distribution functions. The range of values of $r_i(150)$ around the average, defined by the interval $\langle r_i(150)\rangle - \sigma[r_i(150)] \leq r_i(150) \leq \langle r_i(150)\rangle + \sigma[r_i(150)]$, is indicated for each distribution function by a horizontal line through the corresponding tick mark. The reduced mean-square deviations of these distributions, $[\langle r_i^2(N)\rangle - \langle r_i(N)\rangle^2]/\langle r_i(N)\rangle^2$, fall in the range 0.03 to 0.06 and give a further indication of the sharpness of the distributions.

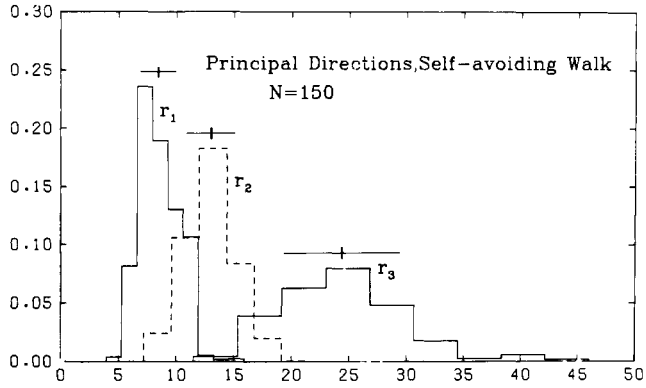

Figure 4. Histograms showing the distribution of values of $r_i(150)$, $i = 1, 2, 3$, for the self-avoiding walk. The abscissa scale is measured in units of the nearest neighbor lattice spacing. The ordinate scale is the fraction of random-walk configurations per unit length of the span for which the span $r_i(150)$ falls in the interval specified on the abscissa. The average values, $\langle r_i(150)\rangle$, associated with the histograms are indicated by vertical tick marks above the peak values. The range of values defined by the interval $\langle r_i(150)\rangle - \sigma[r_i(150)] \leq r_i(150) \leq \langle r_i(150)\rangle + \sigma[r_i(150)]$ is indicated for each histogram by a horizontal line through the associated tick mark.

(ii) The Relative Proportions $\langle r_3(N)\rangle/\langle rN)\rangle$ and $\langle r_2(N)\rangle/\langle r_1(N)\rangle$. The relative proportions, $\rho_3(r;N) = \langle r_3(N)\rangle/\langle r_1(N)\rangle$ and $\rho_2(r;N) = \langle r_2(N)\rangle/\langle r_1(N)\rangle$, are plotted vs. N^{-1} in Figure 5 for both the unrestricted and self-avoiding walks. As in the case of $\rho_3(R;N)$ and $\rho_2(R;N)$, there appears to be a weak dependence of these quantities on N. When the corresponding relative values of the ordered components of the square radius of gyration $\rho_3(S^2;N) = \langle S_3^2(N)\rangle/\langle S_1^2(N)\rangle$ and $\rho_2(S^2;N) = \langle S_2^2(N)\rangle/\langle S_1^2(N)\rangle$ are plotted vs. N^{-1}, a similar weak dependence on N is found; see Figure 6. The results shown in Figure 6 are not new. They merely confirm results obtained for unrestricted random walks by Koyama,[6,7] Solč and Stockmayer,[8] and Solč[9] and results obtained for self-avoiding walks by Mazur, Guttman, and McCrackin.[10] If the N dependence of all these ratios is ignored and the corresponding values obtained for different N are averaged, then the average relative proportions are

$$\overline{\rho_3(r)} = 2.94 \text{ and } \overline{\rho_2(r)} = 1.57 \quad (19)$$

for self-avoiding walks and

$$\overline{\rho_3(r)} = 2.57 \text{ and } \overline{\rho_2(r)} = 1.48 \quad (20)$$

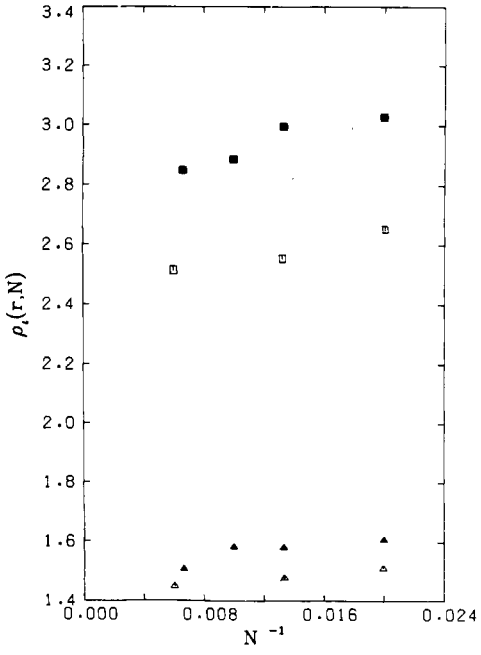

Figure 5. The relative proportions, $\rho_3(r;N) = \langle r_3(N)\rangle/\langle r_1(N)\rangle$ and $\rho_2(r;N) = \langle r_2(N)\rangle/\langle r_1(N)\rangle$, are plotted vs. N^{-1} for both the unrestricted and self-avoiding walks. The squares refer to values of $\rho_3(r,N)$ and the triangles to $\rho_2(r;N)$ while the filled symbols refer to the self-avoiding walk and the open symbols to the unrestricted random walk.

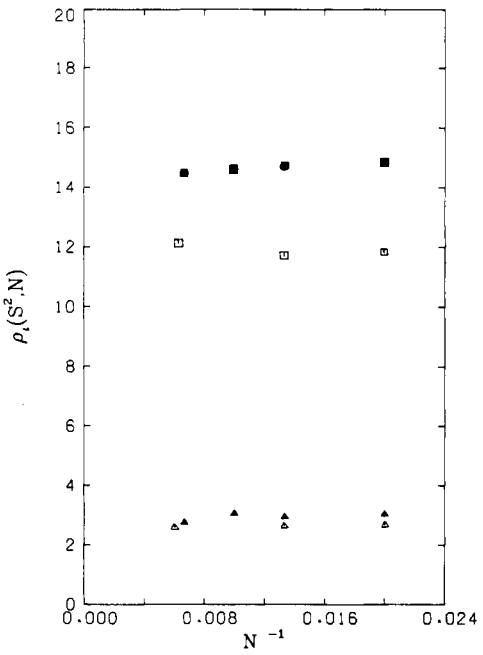

Figure 6. The relative proportions, $\rho_3(S^2;N) = \langle S_3^2(N)\rangle/\langle S_1^2(N)\rangle$ and $\rho_2(S^2;N) = \langle S_2^2(N)\rangle/\langle S_1^2(N)\rangle$, are plotted vs. N^{-1} for both the unrestricted and self-avoiding random walks. The squares refer to values of $\rho_3(S^2;N)$ and the triangles to $\rho_2(S^2;N)$ while the filled symbols refer to the self-avoiding walk and the open symbols to the unrestricted random walk.

for unrestricted walks. The average relative ordered components of the square radius of gyration are

$$\overline{\rho_3(S^2)} = 14.67 \text{ and } \overline{\rho_2(S^2)} = 2.95 \tag{21}$$

for self-avoiding walks and

$$\overline{\rho_3(S^2)} = 11.88 \text{ and } \overline{\rho_2(S^2)} = 2.65 \tag{22}$$

for unrestricted walks.

In order to compare the asymmetry in the shape of a random walk which is implied in the values of the ordered components of the square radius of gyration with the asymmetry which is implied in the values of the spans in the corresponding directions, the above values of $\overline{\rho_3(S^2)}$ and $\overline{\rho_2(S^2)}$ should be compared with the following average values of ratios of average *squares* of spans which are computed from Tables IIA and IIB:

$$\overline{\rho_3(r^2)} = \overline{\langle r_3^2(N)\rangle/\langle r_1^2(N)\rangle} = 6.77$$
$$\overline{\rho_2(r^2)} = \overline{\langle r_2^2(N)\rangle/\langle r_1^2(N)\rangle} = 2.21 \tag{23}$$

for unrestricted walks and

$$\overline{\rho_3(r^2)} = 8.78 \text{ and } \overline{\rho_2(r^2)} = 2.46 \tag{24}$$

for self-avoiding walks. Thus from eq 23 and 24 we find that

$$\overline{\rho_3(S^2)} = 1.67\,\overline{\rho_3(r^2)} \text{ and } \overline{\rho_2(S^2)} = 1.20\,\overline{\rho_2(r^2)} \tag{25}$$

for self-avoiding walks and

$$\overline{\rho_3(S^2)} = 1.75\,\overline{\rho_3(r^2)} \text{ and } \overline{\rho_2(S^2)} = 1.20\,\overline{\rho_2(r^2)} \tag{26}$$

for unrestricted random walks. The disparity between the values of $\overline{\rho_3(S^2)}$ and $\overline{\rho_3(r^2)}$ in eq 25 and 26 can be reconciled in terms of the density distribution of steps inside the right prism which contains a random walk. In particular, $S_i^2(N)$, the ith ordered component of the square radius of gyration given in eq 17, is the average of the squares of the set of all distances of steps measured from the center of gravity of the configuration in the direction $\mathbf{V}_i$, whereas $r_i^2(N)$ is the square of the difference between the largest and smallest coordinates in the same set of distances, $\{x_i'(n)\}$. Detailed examination of this point is contained in section 4.

It was noted in the preceding section that there is a significant anticorrelation between the direction of the smallest span associated with the maximum span $R_3(N)$ and the vector connecting the ends of the polymer chain, $\mathbf{x}(N) = \{x_1(N), x_2(N), x_3(N)\}$, because the mean-square length of $\mathbf{x}(N)$, $\langle x_1^2(N) + x_2^2(N) + x_3^2(N)\rangle$, is larger than either $\langle R_2^2(N)\rangle$ or $\langle R_1^2(N)\rangle$. If we now compare the average values of $\langle r_3(N)\rangle$ in Tables IIA and IIB with the corresponding average values of the maximum span, $\langle R_3(N)\rangle$, in Tables IA and IB and ignore any dependence of the ratios $\langle R_3(N)\rangle/\langle r_3(N)\rangle$ on N, we find that

$$\overline{\langle r_3(N)\rangle/\langle R_3(N)\rangle} = 0.98 \tag{27}$$

for the self-avoiding walk and

$$\overline{\langle r_3(N)\rangle/\langle R_3(N)\rangle} = 0.97 \tag{28}$$

for the unrestricted walk. In view of the near equality between $\langle R_3(N)\rangle$ and $\langle r_3(N)\rangle$, we conclude that the directions associated with $R_3(N)$ and $r_3(N)$ are on the average nearly the same and therefore highly correlated. If the same pair of steps were involved in the two spans, $R_3(N)$ and $r_3(N)$, then the ratios in eq 27 and 28 would be related to average angles between the directions associated with $R_3(N)$ and $r_3(N)$. The angles in question would have the values 11 and 14°, respectively.

If a similar comparison is made between the smallest spans for the two sets of chain-fixed axes by using the data in Tables IA, IB, IIA, and IIB, one obtains

$$\overline{\langle r_1(N)\rangle/\langle R_1(N)\rangle} = 0.91 \tag{29}$$

for self-avoiding walks and

$$\overline{\langle r_1(N)\rangle/\langle R_1(N)\rangle} = 0.92 \tag{30}$$

for unrestricted walks.

4. Density Distribution of Steps Inside Spanning Right Prisms

We now consider the problem of characterizing the density distribution of steps inside the two minimum-size right prisms of sections 2 and 3, $\Pi_R(N)$ and $\Pi_r(N)$, which are associated with the maximum span and with the ordered components of the square radius of gyration, respectively, and which contain the random walk. We introduce two different subdivisions of the right prisms. While each prism can be subdivided in both ways in order to study the density distribution of segments, we limit our discussion to the results of the subdivision of each prism in a single different way.

(i) Density Distribution of Steps in the Prism Based on the Ordered Square Radii of Gyration. Subdivision of $\Pi_r(N)$ into Slabs. The coordinates $x_1'(j), x_2'(j), x_3'(j)$ of the jth step of a random walk, in the coordinate system based on the principal components of the square radius of gyration of that random walk, are obtained from the space-fixed coordinates $x_1(j), x_2(j), x_3(j)$ by the linear transformation in eq 16. The coordinates $x_1'(j), x_2'(j), x_3'(j)$ are measured from the center of gravity of the configuration which is taken as the origin of the x_1', x_2', x_3' coordinate system. In section 3 the procedure for determining the maximum span $r_i(N)$ in the direction of the ith ordered component of the square radius of gyration, S_i^2, is outlined. Once the value of r_i is obtained, the fraction of steps in the random walk whose $x_i'(j)$ coordinate, for $0 \leq j \leq N$, is contained in the interval $0.1(m-1)r_i \leq |x_i'(j)| < 0.1mr_i$ for $1 \leq m \leq 5$ can be determined. Thus, we introduce a central plane through the center of gravity, which is normal to the x_i' axis, and a set of equally spaced parallel planes at distances of $0.1mr_i$ from the central plane. Define a slab as a section of the right prism lying between a pair of adjacent parallel planes. We determine the fraction of the steps lying in pairs of slabs which are equally distant from the central plane. This process is repeated for each of the directions, x_1', x_2', and x_3', and yields three step-density distributions in the form of histograms. The entire foregoing calculation is repeated for each random walk configuration. Average histograms for unrestricted random walks with $N = 50$, 100, and 200 and average histograms for self-avoiding walks with $N = 50$, 75, 100, and 150 are determined. For self-avoiding walks, the forms of the histograms for 150-step random walks are shown in Figure 7 by the solid lines where the ordinate is the fraction of steps in the mth pair of slabs and the abscissa is the slab label, m. The corresponding histograms for 200-step unrestricted random walks are indicated in Figure 7 by the dashed lines. In each case, the total fraction of steps in all slabs is less than one because the central plane passes through the center of gravity of the random walk rather than the geometric center of the spanning right prism. Consequently there is, in general, a portion of the right prism which is not included in the ten slabs. The average fraction of steps which is omitted in this way is indicated by horizontal extensions of the solid- and dashed-line histograms beyond $m = 5$. The root-mean-square average components of the distance between the center of gravity of the random walk and the geometric center of the spanning right prism is less than the slab thicknesses in all cases. For example, in the case of the 150-step self-avoiding random walks, the root-mean-square components of this distance in the directions $i = 1, 2, 3$ are respectively 0.556, 0.838, and 1.584. The corresponding slab thicknesses, which are $0.1r_i$, are: 0.855, 1.289, and 2.437. We have arbitrarily adopted the center of gravity as the center of the step density distribution so that we can correlate the average ordered components of the square radius of gyration, $\langle S_i^2(N) \rangle$, with the corresponding average squares of the spans, $\langle r_i^2(N) \rangle$. The histograms shown in Figure 7 for $N = 150$ are typical of those for other values of N which we have investigated. The differences among the corresponding histograms for self-avoiding walks of different length and the differences among the corresponding histograms for unrestricted walks of different length are small compared to the differences between the two sets of histograms shown in Figure 7. A principal characteristic of both sets of histograms is that the step distribution in the direction of the largest span, $r_3(N)$, is much flatter than the step distribution in the direction of the smallest span, $r_1(N)$. Step distributions for the unrestricted random walk are relatively higher near the central plane than the step densities for the self-avoiding walk.

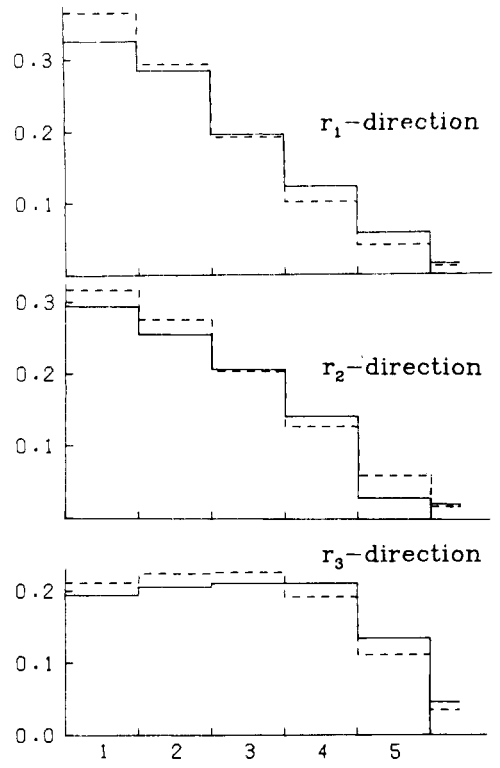

Figure 7. Histograms for 150-step self-avoiding and unrestricted random walks showing the average fraction of steps in pairs of slabs, $1 \leq m \leq 5$. The dissection in ten slabs of equal thickness is carried out in each of the directions based on the ordered square radii of gyration. The solid line refers to the self-avoiding walk and the dashed line to the unrestricted walk. The central cutting plane passes through the center of gravity of the step distribution. The short extension of the histograms beyond $m = 5$ shows the fraction of steps lying outside the slabs.

Finally, for reference purposes, we plot in Figure 8 the analogous histograms for two uniform-density model distributions: (a) uniform density inside a right prism whose edge lengths are r_1, r_2, and r_3; and (b) uniform density inside an ellipsoid whose major axes are r_1, r_2, r_3. In the case of each model, the three histograms corresponding to the three principal directions are identical.

We next derive an approximate relation between an average ordered square component of the radius of gyration and the associated step distribution and span. Rewrite eq 17 as

$$S_i^2(N) = \tfrac{1}{4}r_i^2(N)(N+1)^{-1} \sum_{n=0}^{N} [x_i'(n)]^2 / \tfrac{1}{4}r_i^2(N) \quad (31)$$

and assemble the $N + 1$ terms of the sum in six groups. The first five groups are characterized by the inequalities

$$\left(\frac{m-1}{5}\right)^2 \leq \frac{[x_i'(n)]^2}{\frac{1}{4}r_i^2(N)} \leq \left(\frac{m}{5}\right)^2 \text{ for } 1 \leq m \leq 5 \quad (32)$$

The fraction of terms in the mth group is just the fraction of steps in a pair of slabs and is denoted by $f_i(m;N)$. The sixth

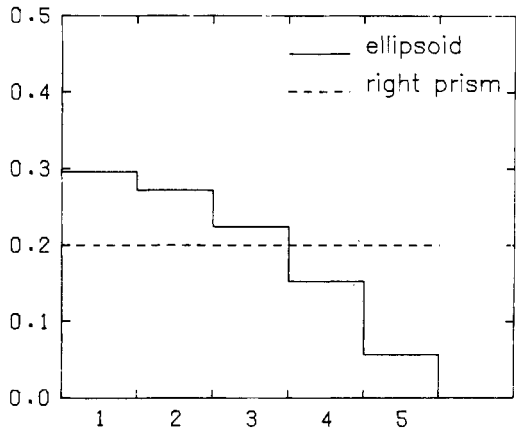

Figure 8. Analogous histograms to those in Figure 7 for two uniform-density models: (a) uniform density inside a right prism whose edge lengths are r_1, r_2, and r_3 and (b) uniform density inside an ellipsoid whose major axes are r_1, r_2, r_3. In each case, the three histograms corresponding to the three principal directions are identical.

group consists of the remaining terms of the sum which lie outside the slabs. The fraction of terms in the sixth group is denoted by $f_{i,0}(N)$. Equation 31 can then be rewritten approximately in terms of these fractions as

$$S_i^2(N) \cong \tfrac{1}{4} r_i^2(N) \left[\sum_{m=1}^{5} f_i(m;N) \left(\frac{m - \tfrac{1}{2}}{5} \right)^2 + f_{i,0}(N) \right] \tag{33}$$

Introduce the average overall walks of length N, and on the right-hand side, replace the average of the products by the products of the averages to obtain

$$\langle S_i^2(N) \rangle \cong \tfrac{1}{4} \langle r_i^2(N) \rangle \left[\sum_{m=1}^{5} \langle f_i(m;N) \rangle \left(\frac{m - \tfrac{1}{2}}{5} \right)^2 + \langle f_{i,0}(N) \rangle \right] \tag{34}$$

Values of $\langle f_i(m;N) \rangle$ and $\langle f_{i,0}(N) \rangle$, given in the form of histograms similar to those in Figure 7 for both unrestricted and self-avoiding walks, can be used to evaluate the term in square brackets in eq 34 and thus can be used to obtain approximate values for the ratio $\langle S_i^2(N) \rangle / \langle r_i^2(N) \rangle$. The values so obtained for this ratio for unrestricted and self-avoiding walks of length $N = 100$ are given in Table III where they are compared with the values computed from the Monte Carlo estimates for $\langle S_i^2(100) \rangle$ and $\langle r_i^2(100) \rangle$ given in Tables IIA and IIB. There is good agreement between the values of the ratio calculated from the approximate eq 34 and that calculated from the Monte Carlo estimates. Equation 34 can be used to account for the relatively large values obtained for the ratios $\langle S_i^2(N) \rangle / \langle S_1^2(N) \rangle$, $i = 2, 3$, by Koyama,[6,7] Solč and Stockmayer,[8] Solč,[9] and Mazur, Guttman, and McCrackin[10] compared with the smaller values which we have obtained for the relative proportions $\langle r_i^2(N) \rangle / \langle r_1^2(N) \rangle$. In particular, the ratio $\langle S_i^2(N) \rangle / \langle S_1^2(N) \rangle$ can be formed using eq 34

$$\frac{\langle S_i^2(N) \rangle}{\langle S_1^2(N) \rangle} = \left[\frac{\sum_{m=1}^{5} \left(\frac{m - 0.5}{5} \right)^2 \langle f_i(m;N) \rangle + \langle f_{i,0}(N) \rangle,}{\sum_{m=1}^{5} \left(\frac{m - 0.5}{5} \right)^2 \langle f_1(m;N) \rangle + \langle f_{1,0}(N) \rangle} \right] \frac{\langle r_i^2(N) \rangle}{\langle r_1^2(N) \rangle} \tag{35}$$

It is clear that the more rapidly $\langle f_1(m;N) \rangle$ falls off with increasing m compared with $f_i(m;N)$, the more the factor in square brackets in (35) exceeds one.

(ii) Distribution of Steps in the Right Prism Based on the Maximum Span. Subdivision into Concentric Ovals. The coordinates $x_1''(j)$, $x_2''(j)$, $x_3''(j)$ of the jth step in a random walk in the coordinate system based on its maximum span are obtained from the space-fixed coordinates $x_1(j)$, $x_2(j)$, $x_3(j)$ by the successive linear transformations 2 and 4, and the center of the spanning right prism can be determined once the steps whose separations are maximal have been determined. As a complement to the analysis of the distribution of steps inside the spanning right prism in terms of slabs, we now analyse the distribution of steps in terms of a set of symmetric, concentric ovals whose centers coincide with the center of the right prism, whose axial directions coincide with the axes of the prism, and whose relative axial dimensions are equal to the relative proportions of the spanning right prism, $R_3(N):R_2(N):R_1(N)$. In particular, we have taken as the general equation of an oval,

$$\left(\frac{|x_1'' - \hat{x}_1''|}{kR_1(N)/2} \right)^n + \left(\frac{|x_2'' - \hat{x}_2''|}{kR_2(N)/2} \right)^n + \left(\frac{|x_3'' - \hat{x}_3''|}{kR_3(N)/2} \right)^n = 1 \tag{36}$$

where, for a given random walk configuration, $\hat{x}_1''$, $\hat{x}_2''$, $\hat{x}_3''$ are the coordinates of the center of the spanning right prism whose edge lengths are $R_1(N)$, $R_2(N)$, and $R_3(N)$. The parameter k is a scale factor such that the case $k = 1.0$ corresponds to the inscribed oval of order n. The volume of the nth order oval for arbitrary k is k^3 times the volume of the inscribed oval of order n. We have considered values of $n = 2$, 3, and 4 in this paper (where $n = 2$ corresponds to the case of the ellipsoid). The volumes, $V^{(n)}$, of the inscribed ovals can be expressed as a fraction of the volume of the spanning right prism, $V^{(n)} = v^{(n)} V_\pi$ where $V_\pi = R_1(N)R_2(N)R_3(N)$. It is shown in Appendix B that $v^{(2)} = 0.523\,60$, $v^{(3)} = 0.712\,07$, and $v^{(4)} = 0.812\,05$. The asymptotic value of $v^{(n)}$ as $n \to \infty$ is also obtained,

$$v^{(n)} \sim 1 - 2.9357 n^{-2} + \ldots \tag{37}$$

Thus, in the limit $n \to \infty$, the nth order oval completely fills the spanning right prism.

In addition to considering several values of n, we have introduced the following set of values of k: $k_1 = 0.50$, $k_2 = 0.65$, $k_3 = 0.80$, $k_4 = 0.95$, and $k_5 = 1.00$. For each value of n, the set

Table III
Values of $\langle S_i^2(100) \rangle / \langle r_i^2(100) \rangle$ Calculated from Step Density Distribution Histograms like Those in Figure 7 Compared with Values Calculated from Monte Carlo Estimates of $\langle S_i^2(100) \rangle$ and $\langle r_i^2(100) \rangle$

	Self-avoiding walk		Unrestricted walk	
i	From histograms	From Monte Carlo estimates	From histograms	From Monte Carlo estimates
1	0.051	0.051	0.046	0.049
2	0.061	0.063	0.054	0.055
3	0.084	0.088	0.077	0.081

Table IV
Monte Carlo Estimates of $\langle g_\pi{}^{(n)}(150)\rangle$, $n = 2, 3, 4$, for Self-Avoiding and Unrestricted Walks

n	Self-avoiding walks	Unrestricted walks
2	0.3274	0.2430
3	0.1426	0.1138
4	0.0817	0.0819

Table V
Average Distribution of Steps in Each of the Fourth Order Oval Shells for 150-Step Self-Avoiding Walks Expressed as a Fraction

i	$\langle g_i{}^{(4)}(150)\rangle$	$\omega_i{}^{(4)}$	k
1	0.1351	0.1013	0.50
2	0.1668	0.1212	0.65
3	0.2531	0.1923	0.80
4	0.2888	0.2798	0.95
5	0.0729	0.1156	1.00
π	0.0817		

of five oval surfaces corresponding to the values of k_i, $1 \leq i \leq 5$, divides the interior of the right prism into six regions $\Omega_i{}^{(n)}$: the central oval, $\Omega_1{}^{(n)}$ (for $k_1 = 0.50$); four oval shells, $\Omega_2{}^{(n)}$, $\Omega_3{}^{(n)}$, $\Omega_4{}^{(n)}$, $\Omega_5{}^{(n)}$; and the remainder of the prism $\Omega_\pi{}^{(n)}$. The volumes of the regions $\Omega_i{}^{(n)}$ and $\Omega_\pi{}^{(n)}$ are denoted by $\omega_i{}^{(n)}V_\pi$ and $\omega_\pi{}^{(n)}V_\pi$, respectively, where the reduced volume

$$\omega_i{}^{(n)} = (k_i{}^3 - k_{i-1}{}^3)v^{(n)}, \quad 1 \leq i \leq 5$$

is expressed as a fraction of the volume of the spanning right prism with $k_0 \equiv 0$ and where

$$\omega_\pi{}^{(n)} = 1 - v^{(n)}$$

For each N-step random-walk configuration, i.e., for each spanning right prism, we have determined the fraction of steps, $g_i{}^{(n)}(N)$, in each of the regions $\Omega_i{}^{(n)}$, $1 \leq i \leq 5$. This histogram, or distribution function, is determined by first evaluating the following function of the coordinates for each of the $N + 1$ lattice points visited in an N-step walk.

$$F_n[x_1''(j), x_2''(j), x_3''(j)] = \left[\left(\frac{|x_1''(j) - \hat{x}_1''|}{R_1(N)/2}\right)^n + \left(\frac{|x_2''(j) - \hat{x}_2''|}{R_2(N)/2}\right)^n + \left(\frac{|x_3''(j) - \hat{x}_3''|}{R_3(N)/2}\right)^n\right]^{1/n}, \quad 0 \leq j \leq N \tag{38}$$

Then the fraction of the set of $N + 1$ values of $F_n \equiv F_n[x_1''(j), x_2''(j), x_3''(j)]$ which fall in each of the intervals, $0 \leq F_n \leq k_1$ and $k_{i-1} \leq F_n \leq k_i$ for $2 \leq i \leq 5$, is determined. These fractions are the desired values of $g_i{}^{(n)}$. The remaining fraction of steps which lie in $\Omega_\pi{}^{(n)}$ is given by

$$g_\pi{}^{(n)}(N) = 1 - \sum_{i=1}^{5} g_i{}^{(n)}(N) \tag{39}$$

The values of $g_i{}^{(n)}(N)$ for $1 \leq i \leq 5$, $n = 2, 3, 4$, and $N = 75, 150$ have been determined for samples of self-avoiding random walks, and average values, $\langle g_i{}^{(n)}(N)\rangle$, have been obtained for these samples. Similar calculations have been performed for unrestricted random walks for $n = 2, 3, 4$ and $N = 50, 100, 150, 200$. Examples of one aspect of these calculations are shown in Table IV where values of $\langle g_\pi{}^{(n)}(150)\rangle$ for self-avoiding and unrestricted walks are tabulated for $n = 2, 3, 4$. The entries for $\langle g_\pi{}^{(4)}(150)\rangle$ are significantly smaller than those for $\langle g_\pi{}^{(3)}(150)\rangle$ and $\langle g_\pi{}^{(2)}(150)\rangle$. Therefore we have limited the presentation of results of the analysis of the segment distribution in terms of ovals to fourth-order ovals. In Table V values of $\langle g_i{}^{(4)}(150)\rangle$, $1 \leq i \leq 5$, and $\langle g_\pi{}^{(4)}(150)\rangle$ are given. In addition, values of the reduced volumes, $\omega_i{}^{(4)}$, of the regions, $\Omega_i{}^{(4)}$, are given in column 3. The last column lists the outer linear dimension of each oval region, $\Omega_i{}^{(4)}$, expressed as a fraction, k_i, of the corresponding dimension of the inscribed oval. We have converted the fractions, $\langle g_i{}^{(4)}(150)\rangle$, listed in Table V to approximate reduced densities by dividing the values of $\langle g_i{}^{(4)}(150)\rangle$ by the corresponding reduced volumes, $\omega_i{}^{(4)}$. These reduced densities,

$$\eta_i{}^{(4)} = \langle g_i{}^{(4)}(150)\rangle / \omega_i{}^{(4)}$$

are plotted vs. $k_i{}^3$ in Figure 9. Calculations of $\langle g_i{}^{(4)}(150)\rangle$ were carried out in batches of 500 walks. The range in the associated values of $\eta_i{}^{(4)}$ obtained from the individual batches is indicated by the dashed vertical line in the k^3 interval associated with each oval shell. Thus it is seen in Figure 9 that $\eta_i{}^{(4)}$ is virtually constant for $i = 1, 2, 3$. Together, these regions comprise approximately one-half of the volume of the inscribed oval while their outer linear dimension is 0.80 times that of the inscribed oval. The horizontal dashed line in Figure 9 indicates the reduced density distribution for a model in which all steps are contained in the inscribed oval and fill the oval uniformly, i.e., $\hat{\eta}_i{}^{(4)} = 1/v^{(4)} \cong 1.234$. Analogous results for the fractional density distribution of segments in the case of the unrestricted random walk are plotted in Figure 10 for the case $N = 150$. As should be expected the fractional density is higher in the center in the case of the unrestricted random walk than in the self-avoiding random walk.

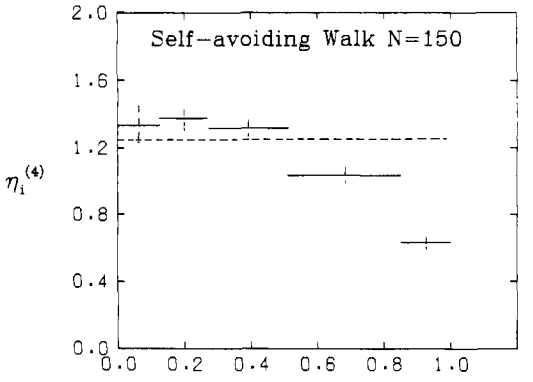

Figure 9. Histogram showing reduced density $\eta_i{}^{(4)}$ plotted vs. $k_i{}^3$ for 150-step self-avoiding walks. The range in the batch average values of $\eta_i{}^{(4)}$ is indicated by the vertical dashed line for each value of i. The horizontal dashed line indicates the reduced density distribution for a model in which all steps are contained in the inscribed oval and fill the oval uniformly.

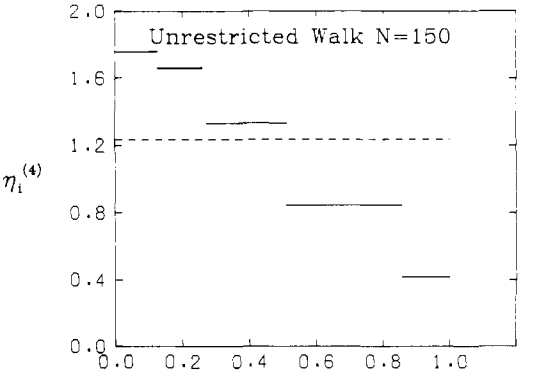

Figure 10. Histogram showing reduced density $\eta_i{}^{(4)}$ plotted vs. $k_i{}^3$ for 150-step unrestricted walks. The horizontal dashed line indicates the reduced density distribution for a model in which all steps are contained in the inscribed oval and fill the oval uniformly.

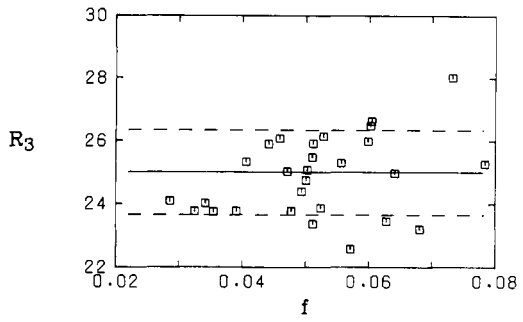

Figure 11. Batch average values of $R_3(150)$ are plotted vs. the statistical weight of the batch of configurations. The horizontal solid line indicates the weighted average values, $\langle R_3(150)\rangle$, and the distance to the parallel dashed lines indicates the magnitude of the root-mean-square dispersion of the batch average values.

5. Concluding Remarks

(1) The ratios of the average largest to average smallest span obtained in this paper, 2.42 for the unrestricted random walk and 2.73 for the self-avoiding random walk, are somewhat smaller than the corresponding values, 2.59 and 3.05, deduced in RMI on the basis of the assumption of an ensemble of identical randomly oriented ellipsoids (oval of order 2). This discrepancy should not be surprising in view of the fact that on the average ¼ to ⅓ of the random walk steps lie outside the inscribed ellipsoid (see entries for oval of order 2 in Table IV). Furthermore, the values of the average spans with respect to space-fixed axes which were used in the ellipsoid model calculation in RMI were $N = \infty$ estimates. Finally, note that we cannot rule out the possibility that in the limit $N \to \infty$ the oval of order $n = 2$ may contain a significantly larger fraction of steps than it does for $N \leq 150$.

(2) In interpreting the results shown in Figures 7, 9, and 10 regarding the average distribution of the steps of a random walk inside its spanning prism, several limitations on the extrapolation to large N behavior should be borne in mind. First, the average prism dimensions for the self-avoiding walk of 150 steps are 25.12, 14.38, and 9.17. When it is recognized that in each random walk at least one contact is made with each face of the spanning prism, then it is seen that in the average spanning prism a minimum of one-half of the 150 steps of the random walk are required merely to move directly from one face of the prism to another. It is only in much longer random walks where the minimum number of steps required to visit all faces of the average spanning prism is small compared to the total number of steps that we may reasonably expect that a limiting asymptotic step density distribution is established. The foregoing condition is $N^{0.61} \ll N$ (or $N^{0.5} \ll N$).

Appendix A. The Bias of Estimates of $\langle R_3(150)\rangle$ in the Method of Rosenbluth and Rosenbluth

The bias of a sample estimate of an average parameter of a self-avoiding walk, such as the span $R_3(N)$, is defined as the difference between the sample estimate and the exact, but unknown, average value of $R_3(N)$ based on all configurations. Bias in a sample estimate obtained by using the method of Rosenbluth and Rosenbluth[11] arises if there is significant correlation between batch average values of $R_3(N)$ and the corresponding statistical weights of the batches of configurations. Such a correlation might arise if open or extended configurations, which are associated with large values of $R_3(N)$, also have large statistical weights. McCrackin[15] and McCrackin, Mazur, and Guttman[13] have outlined a procedure for estimating the magnitude of the bias. Rather than go into complete details here, we present in Figure 11 a correlation diagram in which batch average values of $R_3(150)$ are plotted vs. the corresponding statistical weights of the batches of configurations. Each batch consists of 400 or 500 random-walk configurations as shown in the figure. The solid horizontal line indicates the weighted average of the batch averages and the horizontal dashed lines in Figure 11 indicate the magnitude of the root-mean-square deviation from the weighted average. For the data shown in Figure 11, a calculation following the procedure of McCrackin, Mazur, and Guttman[13] shows the bias to be +0.073, an order of magnitude less than the root-mean-square dispersion in the batch average values of $R_3(150)$.

Appendix B. Volume of Inscribed Oval of Order n

The equation for the inscribed oval of order n when the origin is located at the center of the oval is, according to eq 37,

$$[2|x_1|/R_1(N)]^n + [2|x_2|/R_2(N)]^n + [2|x_3|/R_3(N)]^n = 1 \tag{B1}$$

The volume of this oval is given by the expression

$$V^{(n)} = 8\int_0^{R_3(N)/2} dx_3 \int_0^{\{1-[2x_3/R_3(N)]^n\}^{1/n} R_1(N)/2} dx_1 \times \tfrac{1}{2} R_2(N)\left\{1 - \left(\frac{2x_3}{R_3(N)}\right)^n - \left(\frac{2x_1}{R_1(N)}\right)^n\right\}^{1/n} \tag{B2}$$

The double integral in eq B2 can be transformed and evaluated as the product of two β functions.[20] The final result is

$$V^{(n)} = R_1(N)R_2(N)R_3(N)n^{-2}B(n^{-1}, 1 + n^{-1}) \times B(n^{-1}, 1 + 2n^{-1}) \tag{B3}$$

where

$$B(m,n) = \int_0^1 x^{m-1}(1-x)^{n-1}dx = \Gamma(m)\Gamma(n)/\Gamma(m+n)$$

The final result for $V^{(n)}$ is, after simplification,

$$V^{(n)} = V_\pi \Gamma^3(1 + n^{-1})/\Gamma(1 + 3n^{-1}) \tag{B4}$$

where $V_\pi = R_1(N)R_2(N)R_3(N)$ is the volume of the spanning right prism. When $n = 2$, one obtains the familiar result for the ellipsoid,

$$V^{(2)} = \pi V_\pi/6 \tag{B5}$$

For $n = 3$ and $n = 4$, the values of $V^{(n)}$ are

$$V^{(3)} = 0.712\,07 V_\pi \tag{B6}$$

and

$$V^{(4)} = 0.810\,25 V_\pi \tag{B7}$$

For large n, an asymptotic expression for $V^{(n)}$ can be obtained from eq B4 with the aid of the expansion[21]

$$\ln \Gamma(1 + n^{-1}) = -\ln(1 + n^{-1}) + n^{-1}(1 - \gamma) + \sum_{r=2}^{\infty}(-1)^r[\zeta(r) - 1]n^{-r}/r$$

where

$$\gamma = \lim_{m\to\infty}\left[1 + \frac{1}{2} + \frac{1}{3} + \ldots \frac{1}{m} - \ln m\right] = 0.577\,22\ldots$$

γ is Euler's constant and

$$\zeta(r) = \sum_{k=1}^{\infty} k^{-r}$$

is the Riemann ζ function. The asymptotic value of $V^{(n)}$ for $n \gg 1$ is

$$V^{(n)} \cong V_\pi\{1 - [6\gamma^2 - 3\zeta(2)]n^{-2} + \ldots\} \cong V_\pi\{1 - 2.9357n^{-2} + \ldots\} \tag{B8}$$

Thus, it can be seen that as $n \to \infty$ the volume of the inscribed oval approaches that of the right prism.

References and Notes

(1) R. J. Rubin and J. Mazur, *J. Chem. Phys.*, **63**, 5362 (1975).
(2) W. Kuhn, *Kolloid-Z.*, **68**, 2 (1934).
(3) C. Hollingsworth, *J. Chem. Phys.*, **16**, 544 (1948).
(4) C. Hollingsworth, *J. Chem. Phys.*, **17**, 97 (1949).
(5) J. J. Weidmann, H. Kuhn, and W. Kuhn, *J. Chim. Phys. Phys.-Chim. Biol.*, **50**, 226 (1953).
(6) R. Koyama, *J. Phys. Soc. Jpn.*, **22**, 973 (1967).
(7) R. Koyama, *J. Phys. Soc. Jpn.*, **24**, 580 (1968).
(8) K. Solč and W. H. Stockmayer, *J. Chem. Phys.*, **54**, 2756 (1971).
(9) K. Solč, *J. Chem. Phys.*, **55**, 335 (1971).
(10) J. Mazur, C. M. Guttman, and F. L. McCrackin, *Macromolecules*, **6**, 872 (1973).
(11) M. N. Rosenbluth and A. W. Rosenbluth, *J. Chem. Phys.*, **23**, 356 (1955).
(12) J. Mazur and F. L. McCrackin, *J. Chem. Phys.*, **49**, 648 (1968).
(13) F. L. McCrackin, J. Mazur, and C. M. Guttman, *Macromolecules*, **6**, 859 (1973).
(14) F. L. McCrackin, *J. Chem. Phys.*, **47**, 1980 (1967).
(15) F. L. McCrackin, *J. Res. Natl. Bur. Stand., Sect. B*, **76b**, 193 (1972).
(16) H. E. Daniels, *Proc. Cambridge Philos. Soc.*, **37**, 244 (1941).
(17) H. Kuhn, *Experientia*, **1**, 28 (1945).
(18) M. V. Volkenstein, "Configurational Statistics of Polymeric Chains", Interscience, New York, N.Y., 1963, pp 181 and 183.
(19) In this assumed form of the equation for $\langle R_3(N) \rangle$ we have used the exponent 0.61 which was determined in RMI for the span in a principal lattice direction and which is also consistent with the value obtained by many investigators using Monte Carlo or enumeration–exptrapolation methods. Further, we have arbitrarily assigned the unrestricted random walk value, −0.57, to the constant term in the expression for $\langle R_3(N) \rangle$ because we assume that since the constant term is identical for the average spans of the two kinds of random walks in the case of space-fixed axes that the constant term will also be the same in the asymptotic form for the average *maximum* span of an unrestricted and of a self-avoiding random walk.
(20) M. Abramowitz and I. A. Stegun, Ed., "Handbook of Mathematical Functions", National Bureau of Standards, Washington, D.C., 1964, p 258.
(21) Reference 19, p 256.

Microstructure and Physical Properties of Hydrochlorinated 1,4-Polyisoprene Prepared by Butyllithium in Nonpolar Solvent

A. Tran and J. Prud'homme*

Department of Chemistry, University of Montreal, Montreal, Quebec, Canada H3C 3V1.

Received August 9, 1976

ABSTRACT: Microstructure of partially as well as completely hydrochlorinated 1,4-polyisoprene prepared by butyllithium in nonpolar solvent has been investigated by means of ^1H and ^{13}C NMR spectroscopy. The results show that practically no cyclization occurs in the course of the reaction and that hydrogen chloride adds nearly at random along the polymer chains. The microstructure of the remaining unsaturated units present in the partially hydrochlorinated products is nearly that of polyisoprene indicating equivalent reactivities for the different structural units present in the substrate. The completely hydrochlorinated product is an amorphous material with a T_g 103 K higher than that of the substrate. The variation of T_g is a linear function of the molar percentage of hydrochlorinated units in the polymer.

Hydrochlorination of natural 1,4-polyisoprene such as hevea (*cis*-1,4-polyisoprene) and balata (*trans*-1,4-polyisoprene) has been studied extensively during the last 30 years.[1-5] When in solution, both polymers readily add hydrogen chloride but the reaction is known to produce some amount of cyclized structures along the polymer chain. Nevertheless, hydrochlorinated hevea is a crystallizable material having a syndiotactic type of microstructure; that is, the handedness of the successive quaternary carbon atoms alternates along the polymer chain. In contrast, hydrochlorinated balata does not show any crystallinity. The stereoregularity peculiar to hydrochlorinated hevea has been explained by postulating a chain reaction mechanism specific to cis-1,4 unit sequences.[1,3]

In the present paper we wish to report some results concerning hydrochlorination of highly cis-1,4 well-defined polyisoprene prepared by means of anionic polymerization using butyllithium as initiator and benzene as solvent. This substrate contains 71% of cis-1,4 units, 22% of trans-1,4 units, and only 7% of vinyl units which are essentially of 3,4 structure. Microstructure and physical properties of partially as well as completely hydrochlorinated products have been investigated by means of NMR spectroscopy, x-ray diffraction analysis, and differential scanning calorimetry.

Experimental Section

The polyisoprene sample was prepared in a sealed high-vacuum system using *sec*-butyllithium as initiator and benzene as solvent. Its microstructure determined by ^1H NMR spectroscopy is 71% cis, 22% trans, and 7% 3,4. Its number average molecular weight determined by osmometry is 8.6×10^4.

The hydrochlorination reaction was conducted at 298 K on 300 ml of 1% polyisoprene solution in toluene. The solution was first purged with dry nitrogen to remove any molecular oxygen after which dry hydrogen chloride was bubbled through the reaction system at a pressure slightly above the atmospheric pressure. Aliquots of 50 ml were withdrawn from the system at some intervals from 1 to 24 h. The aliquots were purged with nitrogen and washed with distilled water to remove unreacted hydrogen chloride, after which the products were precipitated into methanol. The molar percentage of unsaturated monomer units remaining in the partially hydrochlorinated samples was determined by ^1H NMR spectroscopy by using the olefinic resonances near 5 ppm.

The ^1H NMR spectra were measured at 100 °C on a Varian HR-220 spectrometer using chlorobenzene as solvent and tetramethylsilane (TMS) as internal reference.

The ^{13}C NMR proton noise-decoupled spectra were measured at room temperature on a Bruker WH-90 spectrometer using deuteriochloroform as solvent and TMS as internal reference. Approximately 5000 pulses with an acquisition time of 0.7 s were used. Flip angle was 30° and spectral sweep width was 6000 Hz.

The glass transition temperatures were measured in duplicate at